

An Analytical Model for Coordinated Multi-Satellite Joint Transmission System

Xiangyu Li¹, Bodong Shang^{1*}

¹Eastern Institute for Advanced Study, Eastern Institute of Technology, Ningbo, 315200, China

Emails: {xyli, bdshang}@eitech.edu.cn

Abstract—Satellite communication is one of the key technologies that is enabling next-generation networks. However, nearest-satellite-supported downlink transmission may not meet a user’s requirements due to limited signal strength, especially in emergent scenarios. In this paper, we investigate a coordinated multi-satellite joint transmission system from a system-level perspective, where a user can be served by multiple satellites to improve its quality-of-service (QoS). Furthermore, we analyze the coverage and rate of a typical user in the joint transmission system. Simulation and numerical results show that the introduced system achieves a higher coverage probability than the traditional nearest-satellite-supported network. Moreover, a user’s ergodic rate can be maximized by selecting an appropriate number of serving satellites.

Keywords—Satellite communication, non-terrestrial networks, coverage probability, achievable data rate.

I. INTRODUCTION

Satellite communication (SatCom) is playing an increasingly significant role in today’s fifth generation (5G) and beyond 5G (B5G) wireless communication systems. Due to its deployment locations and characteristics in space environment, the satellite system is able to provide pervasive and seamless network coverage as a complement for terrestrial networks, where unavoidable blockages and limitations can be largely overcome. Apart from the geostationary orbit (GEO) satellites, low-earth orbit (LEO) satellites, which are deployed below the altitude of 2,000 km and faced with fewer challenges such as long transmission delay and power consumption [1], can also serve as ideal candidates for SatCom.

However, in a nearest-satellite-supported area where higher data rates are needed by users, current satellite network structure may not be sufficient. The terrestrial users may experience poor communication conditions, especially in emergent scenarios or when satellites are in a sparse area, which leads to severe scattering of transmitted signals. Hence, it is imperative to model and analyze a coordinated multi-satellite joint transmission system, where a user can be simultaneously served by multiple satellites to overcome the limitations of poor desired signal strength and severe co-channel interference in traditional nearest-satellite-supported network.

Many previous papers have studied SatCom systems. The downlink coverage and rate analysis in LEO satellite network is investigated in [2]. In [3], satellite gateways are deployed on the ground to serve as a relay between LEO satellite and users. The use of Poisson point processes (PPP) is analyzed in [4], where tractable expressions for coverage in downlink satellite

networks are obtained. In [5], the authors studies the satellite-to-airplane system where each airplane is served by the nearest satellite. Related works [6], [7] only use one LEO satellite as a single component out of the terrestrial networks. Nevertheless, these above works concentrate on a typical user served only by the nearest LEO satellite instead of satellite coordination. The coverage performance in cooperative LEO satellite networks is investigated in [8]; however, the use of order statistics makes the derivation complex for multiple satellites, and the corresponding achievable data rate remains unknown. Moreover, centralized and distributed massive multiple-input multiple-output-enabled LEO satellites have been studied in [9], [10]; however, the location randomness of satellites and users in these works is ignored and the network nodes are limited to a certain small area-of-interest.

Motivated by the aforementioned observations, we derive the analytical expressions and analyze the performance of the coordinated multi-satellite joint transmission system in terms of its coverage probability and achievable data rate. It is revealed that the introduced system can significantly improve the coverage probability and achievable data rate of users on the earth under the scattering environment.

II. SYSTEM MODEL

A coordinated multi-satellite joint transmission system comprising of M satellite APs (SAPs) in the space and K user terminals (UTs) on the ground is investigated. We assume that SAPs are coordinated by a central base station (BS) which is either on the ground or on an existing SAP with enough power and computing capabilities [8].

A. Network Model

The signal propagation is affected by path-loss attenuation and small-scale fading. Let the channel coefficient between m th SAP and k th user to be $g_{mk} = \beta_{mk}^{1/2} h_{mk}$. Using a log-distance model, the path-loss attenuation can be modeled as $\beta_{mk} = d_{mk}^{-\alpha}$ with the distance d_{mk} in between. We consider the Rayleigh small-scale fading channel for ease of analysis [2], i.e., $h_{mk} \sim \mathcal{CN}(0, 1)$. This can be reasonable when it refers to a drastic and complex fading environment on the earth, such as in canyon, wooded mountains, and terrestrial-communications-unavailable urban environments during emergencies, where the received signals will be affected by severe multi-path distortion. More sophisticated fading models will be investigated in future work. A typical UT, i.e. k th UT located

at the top of the earth, is selected for the sake of analysis simplicity. All SAPs in typical UT's connected range, as defined in the following section, simultaneously serve the typical UT, while those outside the range will bring interference to its received signal. We assume that UTs associated with the same SAP are assigned orthogonal sub-channels to avoid mutual interference in proximity.

Let q_k be the normalized dummy or data symbol intended for the k th UT such that $\mathbb{E}\{|q_k|^2\} = 1$, and denote Φ_k , Φ_k^S , and Φ_k^I as the sets of all SAPs above UT's horizon line, serving SAPs, and interfering SAPs, respectively. As shown in Fig. 1, serving SAPs make the typical UT's elevation angle greater than ζ , and other SAPs above the typical UT's horizon are interfering SAPs. The signals received by k th UT is

$$\begin{aligned} r_k &= \sqrt{P_d} \sum_{m \in \Phi_k} \beta_{mk}^{1/2} h_{mk} q_k + w_{dk} \\ &= \underbrace{\sqrt{P_d} \sum_{m \in \Phi_k^S} d_{mk}^{-\alpha/2} h_{mk} q_k}_{\text{DS}_k} \\ &\quad + \underbrace{\sqrt{P_d} \sum_{m \in \Phi_k^I} d_{mk}^{-\alpha/2} h_{mk} q_k + w_{dk}}_{\text{IS}_k}, \end{aligned} \quad (1)$$

where P_d is the maximum normalized satellite transmit power and $w_{dk} \sim \mathcal{CN}(0, 1)$ is the additive white Gaussian noise (AWGN). Moreover, DS_k and IS_k represent the desired signal and interfering signal received at k th UT.

B. Spatial Distribution

We model the randomly deployed SAPs on the surface of a sphere in \mathbb{R}^3 centering at the origin $\mathbf{0} \in \mathbb{R}^3$, with radius R_S . All SAPs are distributed according to a homogeneous spherical Poisson point process (SPPP). The probability of having n nodes within the sphere $\mathbb{S}_{R_S}^2$ is given by

$$\mathbb{P}\{N(\mathbb{S}_{R_S}^2) = n\} = \frac{(4\pi R_S^2 \lambda_S)^n}{n!} \exp(-4\pi R_S^2 \lambda_S), \quad (2)$$

where $N(\mathbb{S}_{R_S}^2)$ denotes the number of SAPs in the sphere $\mathbb{S}_{R_S}^2$ and λ_S is the density of SAPs. Similarly, define the surface of the earth to be $\mathbb{S}_{R_E}^2$ with radius $R_E (< R_S)$. All UTs are also randomly distributed on the surface with density λ_U following the homogeneous SPPP. Moreover, the distribution of the SAPs and the UTs are independent on each other due to the movement of LEO satellites and UTs.

III. PERFORMANCE ANALYSIS

A. Statistical Properties

A sketch of modeling and related parameters for analyzing the typical UT have been depicted in Fig. 1. The typical UT is simultaneously served by SAPs in its connected range. As shown in this figure, the angle ζ represents the elevation angle from the typical UT's horizon line, while η is its complementary angle in the same plane. The connected range is the area within the cone angle of 2η .

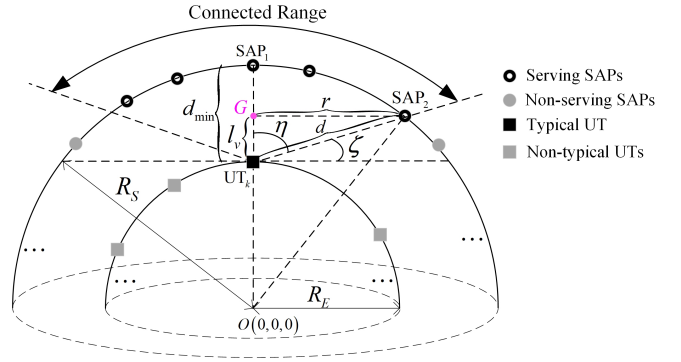


Fig 1: A sketch of coordinated multi-satellite joint transmission system.

Lemma 1. *The cumulative distribution function (CDF) of the distance D from any one of the serving SAPs to the typical UT with the angle η is given in (3) at the top of next page, where $\eta \in [0, \frac{\pi}{2}]$, and the corresponding probability density function (PDF) is given by*

$$f_D(d) = \frac{d}{R_E(R_S - R_E \sin^2 \eta - \sqrt{R_S^2 - R_E^2 \sin^2 \eta} \cos \eta)}, \quad (4)$$

for $(R_S - R_E) \leq d \leq \sqrt{R_S^2 - R_E^2 \sin^2 \eta} - R_E \cos \eta$ while $f_D(d) = 0$ otherwise.

Proof: The distance from any one of the serving SAPs to the typical UT in terms of the angle η needs first to be given. In Fig. 1, consider one triangle formed by SAP_2 , point G and UT_k , and the other by SAP_2 , point G and original point O . Among known parameters R_S , R_E , η and θ , by using geometrical relationships, i.e. $r = R_S \sin \theta = d \sin \eta$ and $R_S \cos \theta = R_E + d \cos \eta$, the distance can be represented as

$$d = \sqrt{R_S^2 - R_E^2 \sin^2 \eta} - R_E \cos \eta. \quad (5)$$

Moreover, the CDF of the distance D from any one of SAP on the outer sphere to the typical UT is provided in [2] as

$$F_D(d) = \begin{cases} 0, & 0 < d < R_E \\ \frac{d^2 - (R_S - R_E)^2}{4R_E R_S}, & R_E < d < (R_E + R_S) \\ 1, & d > (R_E + R_S) \end{cases} \quad (6)$$

By multiplying the middle-case CDF expression in (6) with a scaling factor $\varpi = \frac{2R_S}{R_S - R_E \sin^2 \eta - \cos \eta \sqrt{R_S^2 - R_E^2 \sin^2 \eta}}$, the CDF in (3) can be obtained and corresponding PDF is obtained via derivation, which completes the proof. \square

Lemma 2. *The lowest altitude for the serving SAPs of the typical UT is given by*

$$l_v(\eta) = \begin{cases} \cos^2 \eta \left(\sqrt{R_E^2 + \frac{R_S^2 - R_E^2}{\cos^2 \eta}} - R_E \right), & 0 \leq \eta < \frac{\pi}{2} \\ 0, & \eta = \frac{\pi}{2} \end{cases} \quad (7)$$

Then, the maximum distance from a serving SAP to the typical UT is $\frac{l_v}{\cos \eta}$ for $0 \leq \eta < \frac{\pi}{2}$, and $\sqrt{R_S^2 - R_E^2}$ for $\eta = \frac{\pi}{2}$.

Proof: For previous two triangles, by taking trigonometric function $l_v = r \tan \eta$ and Pythagorean theorem $R_S^2 = r^2 +$

$$F_D(d) = \begin{cases} 0, & 0 < d < (R_S - R_E) \\ \frac{d^2 - (R_S - R_E)^2}{2R_E(R_S - R_E \sin^2 \eta - \sqrt{R_S^2 - R_E^2 \sin^2 \eta} \cos \eta)}, & (R_S - R_E) \leq d \leq \sqrt{R_S^2 - R_E^2 \sin^2 \eta} - R_E \cos \eta \\ 1, & d > \sqrt{R_S^2 - R_E^2 \sin^2 \eta} - R_E \cos \eta \end{cases} \quad (3)$$

$(l_v + R_E)^2$, the lowest altitude for serving SAPs is given as

$$l_v(\eta) = \cos^2 \eta \left(\sqrt{R_E^2 + \frac{R_S^2 - R_E^2}{\cos^2 \eta}} - R_E \right), \quad (8)$$

for $0 \leq \eta < \frac{\pi}{2}$, while $l_v(\eta) = 0$ is obvious for $\eta = \frac{\pi}{2}$, which completes the proof. \square

Lemma 3. *The average number of ground UTs that are within the serving area of an SAP is given by*

$$N_U = 2\pi R_E \lambda_U \left(R_E - \frac{R_E^2}{R_S} \sin^2 \eta - \frac{R_E \sqrt{R_S^2 - R_E^2 \sin^2 \eta} \cos \eta}{R_S} \right). \quad (9)$$

Proof: As shown in Fig. 2, the typical UT is at the top of the inner semicircle which represents the surface of the earth, while a certain SAP is on the outer semicircle which represents LEO. The maximum distance from a serving SAP of the typical UT to its coverage area is given in (5) in Lemma 1, as has been marked as d_{mk} in the figure. Consider the triangle

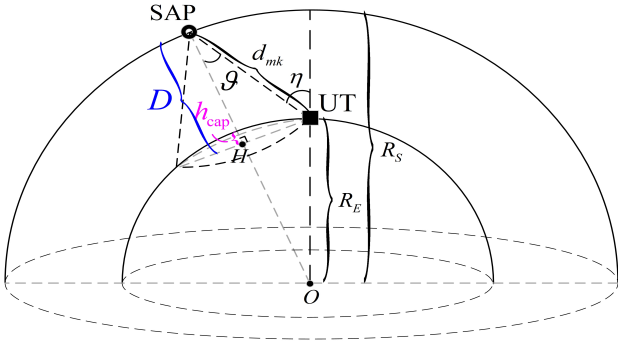


Fig 2: Statistical Properties for coverage area of a satellite.

formed by SAP, typical UT and origin O . Based on the cosine theorem, we have the relationship $\cos \vartheta = \frac{R_S^2 - R_E^2 + d^2}{2R_S d}$. In another triangle formed by SAP, typical UT and point H , by inserting d and $\cos \vartheta$, we have distance $D = d \cos \vartheta$ shown in the figure given by

$$D = R_S - \frac{R_E^2}{R_S} \sin^2 \eta - \frac{R_E \sqrt{R_S^2 - R_E^2 \sin^2 \eta} \cos \eta}{R_S}. \quad (10)$$

The height of the spherical cap can be written as $h_{\text{cap}} = D + R_E - R_S$. Using surface area formula for the spherical cap $S_{\text{service}} = 2\pi R_E h_{\text{cap}}$, the average number of UTs in coverage of SAP is written as in (9), which completes the proof. \square

B. Coverage and Rate Analysis

Definition 1: If the downlink signal-to-interference-plus-noise-ratio (SINR) from its serving SAPs is higher than the threshold value γ_{th} , this typical UT is in the coverage. With the received signal in (1), the SINR of the typical UT is given by

$$\text{SINR}_k = \frac{P_d G_t \beta_0 \left| \sum_{m \in \Phi_k^S} d_{mk}^{-\alpha/2} h_{mk} \right|^2}{P_d G_t \sum_{m \in \Phi_k^I} \beta_0 d_{mk}^{-\alpha} |h_{mk}|^2 + \sigma_{n_0}^2}, \quad (11)$$

where G_t is the satellite antenna gain, β_0 is the path-loss at a reference distance, and $\sigma_{n_0}^2$ is the variance of AWGN. The coverage probability of the typical UT is written as

$$\begin{aligned} & \mathbb{P}_k^{\text{cov}}(\gamma_{th}; \lambda_S, \lambda_U, R_S, P_d, G_t) \\ &= \mathbb{P} \{ \text{SINR}_k > \gamma_{th} \} \\ &= \mathbb{P} \left\{ \frac{P_d G_t \beta_0 \left| \sum_{m \in \Phi_k^S} d_{mk}^{-\alpha/2} h_{mk} \right|^2}{P_d G_t \sum_{m \in \Phi_k^I} \beta_0 d_{mk}^{-\alpha} |h_{mk}|^2 + \sigma_{n_0}^2} > \gamma_{th} \right\} \\ &= \mathbb{P} \left\{ \left| \sum_{m \in \Phi_k^S} d_{mk}^{-\alpha/2} h_{mk} \right|^2 \right. \\ &\quad \left. > \gamma_{th} \sum_{m \in \Phi_k^I} d_{mk}^{-\alpha} |h_{mk}|^2 + \frac{\gamma_{th} \sigma_{n_0}^2}{P_d G_t \beta_0} \right\}. \end{aligned} \quad (12)$$

Theorem 1. *The coverage probability of the system is given in (13) at the top of next page.*

Proof: Consider the typical spherical cap \mathcal{A}_r in [4], i.e.

$$|\mathcal{A}_r| = 2\pi \left(R_S - R_E - \frac{(R_S^2 - R_E^2) - r^2}{2R_E} \right) R_S, \quad (14)$$

where r is the distance from an SAP to the typical UT. Denote $\frac{1}{\lambda_R} = \sum_{m \in \Phi_k^S} d_{mk}^{-\alpha}$ as the sum of channels between the typical UT and its serving SAPs. Taking the derivation $\frac{\partial |\mathcal{A}_r|}{\partial r} = 2 \frac{R_S}{R_E} \pi r$, we further represent the sum of channels as

$$\begin{aligned} \mathbb{E} \left\{ \frac{1}{\lambda_R} \right\} &= \mathbb{E} \left\{ \sum_{m \in \Phi_k^S} d_{mk}^{-\alpha} \right\} = \lambda_S \frac{\partial |\mathcal{A}_r|}{\partial r} \int_{r_{S,\min}}^{r_{S,\max}} r^{-\alpha} dr \\ &= 2 \frac{R_S}{R_E} \pi \lambda_S \int_{r_{S,\min}}^{r_{S,\max}} r^{1-\alpha} dr, \end{aligned} \quad (15)$$

where $r_{S,\min} = R_S - R_E$, $r_{S,\max} = \sqrt{R_S^2 - R_E^2 \sin^2 \eta} - R_E \cos \eta$. Then, by defining $I_k = \sum_{m \in \Phi_k^I} d_{mk}^{-\alpha} |h_{mk}|^2$, the

$$\mathbb{P}_k^{\text{cov}}(\gamma_{th}; \lambda_S, \lambda_U, R_S, P_d, G_t) \approx \exp\left(-\pi\lambda_S \frac{R_S}{R_E} s^{\frac{2}{\alpha}} \int_{s^{-\frac{2}{\alpha}} r_{I,\min}^2}^{s^{-\frac{2}{\alpha}} r_{I,\max}^2} 1 - \frac{1}{1+u^{-\alpha/2}} du - \frac{s\sigma_{n_0}^2}{P_d G_t \beta_0}\right)$$

where $s = \lambda_R \gamma_{th}$,

$$r_{I,\min} = \sqrt{R_S^2 - R_E^2 \sin^2 \eta} - R_E \cos \eta, r_{I,\max} = \sqrt{R_S^2 - R_E^2},$$

$$r_{S,\min} = R_S - R_E, r_{S,\max} = \sqrt{R_S^2 - R_E^2 \sin^2 \eta} - R_E \cos \eta.$$
(13)

coverage probability can be written as

$$\begin{aligned} & \mathbb{P}_k^{\text{cov}}(\gamma_{th}; \lambda_S, \lambda_U, R_S, P_d, G_t) \\ &= \mathbb{P}_k \left\{ \left| \sum_{m \in \Phi_k^S} d_{mk}^{-\frac{\alpha}{2}} h_{mk} \right|^2 > \gamma_{th} I_k + \frac{\gamma_{th} \sigma_{n_0}^2}{P_d G_t \beta_0} \right\} \\ &\stackrel{(a)}{=} \mathbb{E}_{\Phi_k^I} \left\{ \exp \left[-\frac{1}{\sum_{m \in \Phi_k^S} d_{mk}^{-\alpha}} \left(\gamma_{th} I_k + \frac{\gamma_{th} \sigma_{n_0}^2}{P_d G_t \beta_0} \right) \right] \right\} \\ &\stackrel{(b)}{\approx} \mathbb{E}_{\Phi_k^I} \left\{ \exp \left[-\lambda_R \left(\gamma_{th} I_k + \frac{\gamma_{th} \sigma_{n_0}^2}{P_d G_t \beta_0} \right) \right] \right\} \\ &\stackrel{(c)}{=} \mathbb{E}_{\Phi_k^I} \left\{ \mathcal{L}_{I_k}(s) \exp \left(-\frac{s\sigma_{n_0}^2}{P_d G_t \beta_0} \right) \right\}, \end{aligned}$$
(16)

where (a) follows from $\left| \sum_{m \in \Phi_k^I} d_{mk}^{-\alpha/2} h_{mk} \right|^2 \sim \exp(\lambda_R)$; in (b) the approximation holds due to (15); (c) holds true because of the Laplace transform (LT) of the interference, i.e., $\mathcal{L}_I(s) = \mathbb{E} \{ e^{-sI} \}$, and let $s = \lambda_R \gamma_{th}$. For a given γ_{th} , denote $s = \lambda_R \gamma_{th}$, the LT of the interference is given by

$$\begin{aligned} & \mathcal{L}_{I_k}(s) \\ &= \mathbb{E}_{\Phi_k^S, h} \{ \exp(-sI_k) \} \\ &= \mathbb{E}_{\Phi_k^S} \left\{ \prod_{m \in \Phi_k^I} \mathbb{E}_h \left\{ \exp(-s |h_{mk}|^2 d_{mk}^{-\alpha}) \right\} \right\} \\ &= \mathbb{E}_{\Phi_k^S, |h|^2} \left\{ \prod_{m \in \Phi_k^I} \frac{1}{1 + s d_{mk}^{-\alpha}} \right\} \\ &= \exp \left(-\lambda_S \int_{d \in \mathcal{A}_k^I} 1 - \frac{1}{1 + s d_{mk}^{-\alpha}} dr \right) \\ &= \exp \left(-\pi\lambda_S \frac{R_S}{R_E} s^{\frac{2}{\alpha}} \int_{s^{-\frac{2}{\alpha}} r_{I,\min}^2}^{s^{-\frac{2}{\alpha}} r_{I,\max}^2} 1 - \frac{1}{1 + u^{-\alpha/2}} du \right), \end{aligned}$$
(17)

where $r_{I,\min} = \sqrt{R_S^2 - R_E^2 \sin^2 \eta} - R_E \cos \eta$, $r_{I,\max} = \sqrt{R_S^2 - R_E^2}$. Invoke (17) into (16), we finish the proof. \square

Theorem 2. *The achievable data rate of the system is*

$$R_k = \frac{B}{N_U} \int_0^\infty \exp \left(-\pi\lambda_S \frac{R_S}{R_E} s^{\frac{2}{\alpha}} \int_{s^{-\frac{2}{\alpha}} r_{I,\min}^2}^{s^{-\frac{2}{\alpha}} r_{I,\max}^2} 1 - \frac{1}{1 + u^{-\alpha/2}} du - \frac{s\sigma_{n_0}^2}{P_d G_t \beta_0} \right) dt,$$
(18)

where B is the bandwidth, $s = \lambda_R(2^t - 1)$, and N_U is the average number of UTs served by each SAP given in (9).

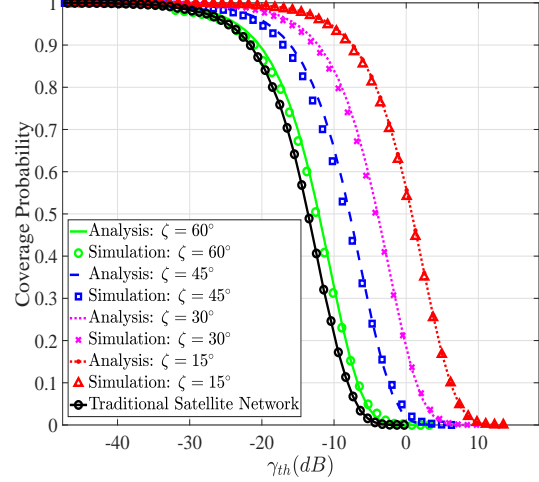


Fig 3: Coverage probability with different elevation angles and comparison with traditional satellite network.

Proof: Since $\mathbb{E}\{X\} = \int_0^\infty \mathbb{P}\{X > x\} dx$ for $X > 0$,

$$\mathbb{E} \{ \log_2(1 + \text{SINR}_k) \} = \int_0^\infty \mathbb{P} \{ \text{SINR}_k > 2^t - 1 \} dt.$$
(19)

Take $\gamma_{th} = 2^t - 1$ and insert (13), we complete this proof. \square

IV. SIMULATIONS AND NUMERICAL RESULTS

In simulations, a number of UTs are scattered on the surface of the earth with a radius of 6371.393 km while SAPs are distributed on the orbit of 500 km above the earth, both according to SPPP. The densities of UTs and SAPs are 10^{-6} per km^2 and 5×10^{-6} per km^2 , respectively. The coverage probability comparisons are obtained by using Monte Carlo simulations for 10,000 times. The path-loss factor $\alpha = 2$.

Fig. 3 demonstrates the coverage probability for various threshold values from -40 dB to 20 dB. Simulations verify our derived analytical results. With a smaller elevation angle, UT can have a higher coverage probability under the same threshold value, which is in line with our intuition. Moreover, these results are compared with those in the traditional satellite network where a typical user is served by the nearest satellite. Better performances can be achieved by using the CFLS network compared with the traditional satellite system. This is meaningful for UTs in emergent circumstances when terrestrial networks are temporarily out of use.

Fig. 4 compares the achievable downlink data rate under different densities of UTs. We observe that in each case there exists an optimal elevation angle for maximal achievable data

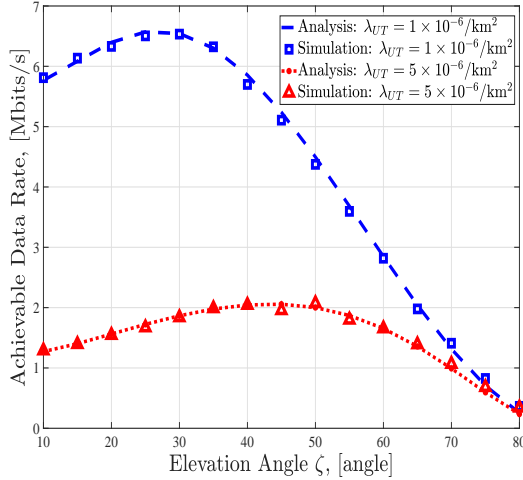


Fig 4: Achievable data rate against elevation angle under different densities of UTs. The altitude and density of SAP are $h = 500$ km, $\lambda_{SAP} = 5 \times 10^{-6} / \text{km}^2$, respectively.

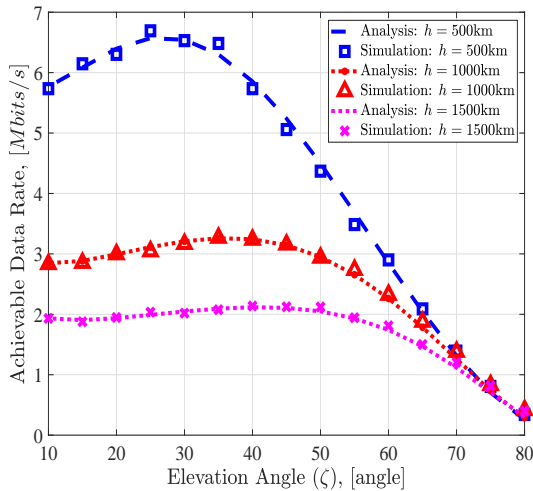


Fig 5: Achievable data rate against elevation angle under various SAPs' altitudes. Densities of UT and SAP are $1 \times 10^{-6} / \text{km}^2$ and $5 \times 10^{-6} / \text{km}^2$, respectively.

rate. Along with the increase of UT density, comes the increase of the elevation angle. The maximal achievable data rate also decreases when the UT density increases. This is because an SAP will need to serve more UTs with fixed bandwidth.

The achievable downlink data rate for different altitudes of SAPs is shown Fig. 5. We notice that the altitude of SAPs has a large influence on both achievable data rate and optimal elevation angle. For instance, when SAP altitude is 500 km, the maximal achievable data rate is 6.6 Mbits/s under $\zeta = 25^\circ$. The maximal achievable data rate drops to 3.3 Mbits/s under $\zeta = 35^\circ$ when SAP altitude is 1,000 km. Note that the optimal elevation becomes less evident as the SAP altitude increases.

In Fig. 6, the spectral efficiency (SE) of the typical UT is also compared under different altitudes of SAPs. It is observed that SE increases with a higher SAP altitude. This is because that the decrease of interference power dominates the increase of desired signal power. The data rate decreases with a higher altitude due to reduction of bandwidth for UT.

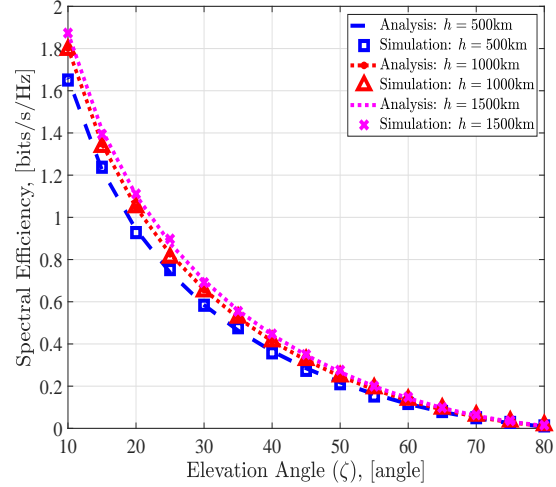


Fig 6: Spectral efficiency against elevation angle under different altitudes of SAPs, where $\lambda_{UT} = 1 \times 10^{-6} / \text{km}^2$ and $\lambda_{SAP} = 5 \times 10^{-6} / \text{km}^2$.

V. CONCLUSION

In this paper, we investigated the coordinated multi-satellite joint transmission system. We analyzed the performance by considering the elevation angles, satellite altitudes and distribution densities of both SAPs and UTs. Simulations and numerical results show that the introduced system improves the coverage 2-15 dB compared to the traditional nearest-satellite-supported network. Moreover, the higher altitude of SAPs brings the lower achievable data rate whilst the higher spectral efficiency given the total number of satellites. Besides, we can obtain an optimal elevation angle to maximize the average achievable data rate of the typical user.

REFERENCES

- [1] B. Shang, Y. Yi, and L. Liu, "Computing over space-air-ground integrated networks: Challenges and opportunities," *IEEE Network*, vol. 35, no. 4, pp. 302–309, 2021.
- [2] N. Okati, T. Riihonen, D. Korpi, I. Angervuori, and R. Wichman, "Downlink coverage and rate analysis of low earth orbit satellite constellations using stochastic geometry," *IEEE Transactions on Communications*, vol. 68, no. 8, pp. 5120–5134, 2020.
- [3] A. Talgat, M. A. Kishk, and M.-S. Alouini, "Stochastic geometry-based analysis of leo satellite communication systems," *IEEE Communications Letters*, vol. 25, no. 8, pp. 2458–2462, 2021.
- [4] J. Park, J. Choi, and N. Lee, "A tractable approach to coverage analysis in downlink satellite networks," *IEEE Transactions on Wireless Communications*, vol. 22, no. 2, pp. 793–807, 2022.
- [5] X. Wang, N. Deng, and H. Wei, "Coverage and rate analysis of leo satellite-to-airplane communication networks in terahertz band," *IEEE Transactions on Wireless Communications*, pp. 1–1, 2023.
- [6] C. Liu, W. Feng, Y. Chen, C.-X. Wang, and N. Ge, "Cell-free satellite-uav networks for 6g wide-area internet of things," *IEEE journal on selected areas in communications*, vol. 39, no. 4, pp. 1116–1131, 2020.
- [7] J. Li, L. Chen, P. Zhu, D. Wang, and X. You, "Satellite-assisted cell-free massive mimo systems with multi-group multicast," *Sensors*, vol. 21, no. 18, p. 6222, 2021.
- [8] B. Shang, X. Li, C. Li, and Z. Li, "Coverage in cooperative leo satellite networks," *Journal of Communications and Information Networks*, vol. 8, no. 4, pp. 329–340, 2023.
- [9] L. You, K.-X. Li, J. Wang, X. Gao, X.-G. Xia, and B. Ottersten, "Massive mimo transmission for leo satellite communications," *IEEE Journal on Selected Areas in Communications*, vol. 38, no. 8, pp. 1851–1865, 2020.
- [10] M. Y. Abdelsadek, G. K. Kurt, and H. Yanikomeroglu, "Distributed massive mimo for leo satellite networks," *IEEE Open Journal of the Communications Society*, vol. 3, pp. 2162–2177, 2022.